Additional results

The F_1 model correctly predicts the ATP synthesis rate when torque is applied to the γ-shaft

The hydrolysis-driven motor investigated by the Japanese group (Noji, et al., 1997; Yasuda, et al., 1998) did not contain the ε subunit. Therefore, some of the interactions between rotor and stator that are known to be important were missing in their experiments. These interactions appear unnecessary in the hydrolysis direction, and so we modeled the elastic potentials as simply as possible to reproduce their results. However, in order to perform correctly in the synthesis direction, the rotation of γ must be coordinated with the binding of reactants and the release of product. First, the rotation of γ must be retarded until ADP and phosphate are *sequentially* bound at the catalytic site. Otherwise, rotation will frequently bypass the phosphate binding sector resulting in a wasted rotation. Second, the catalytic site must trap ATP for release. That is, since ATP is in equilibrium with ADP and P_i with $K_{eq} \sim 1$, there must be a mechanism to alter the catalytic site so that ATP is favored as rotation of γ applies strain to the site to open it up. The shapes of the potentials in Figure 3b in the text do not ensure this sequence of events, so they will not work properly in the synthesis direction. Therefore, we investigated what alterations in the potentials would allow the F_1 model to synthesize ATP at the appropriate rate when a torque of ~ 45 pN-nm is applied to the γ–shaft, the amount necessary to release the tightly bound nucleotide from the catalytic site of a β subunit (Elston, et al., 1998).

We found that adding two 'bumps' to the **DP** ($ADP{\bullet}P_i$) and **T** (ATP) curves as shown in Figure 1 accomplished the task. The sequence of events is enumerated in the figure caption. The shape of the **E** (Empty) potential retards rotation until ADP is bound. The barrier on **D** (ADP) potential for trapping phosphate could be supplied by the ε-subunit, which is absent in the hydrolysis experiments. The shapes of the **DP** ($ADP{\bullet}P_i$) and **T** (ATP) potentials trap nucleotide in the ATP form until it can dissociate into solution, lest the site release reactants rather than product. Interestingly, the modified potentials shown in Figure 1 drive the motor in the hydrolysis direction somewhat more efficiently than those in Figure 3b in the text. Figure 2a shows that ATP is produced at the observed rate when this torque is applied to the γ subunit.

At physiological conditions, the transmembrane protonmotive force in mitochondria is 220 ~ 230 mV (Stryer, 1995). The observed maximum ATP synthesis rate at saturated oxygen supply is about 400 ATP/s/F_1 (Boyer, 1993; Matsuno-Yagi, et al., 1986). During ATP synthesis, the rotary torque applied to the γ shaft of F_1 is generated in F_0 by a protonmotive force. To simulate ATP synthesis rate as a function of the protonmotive force, we combined the F_1 model in this study with the F_0 model in the previous study (Elston, et al., 1998) by constraining the F_1 and F_0 to rotate at the same rate. In Figure

2b, the correct ATP synthesis rate is achieved when the protonmotive force across F_o is in the physiological range.

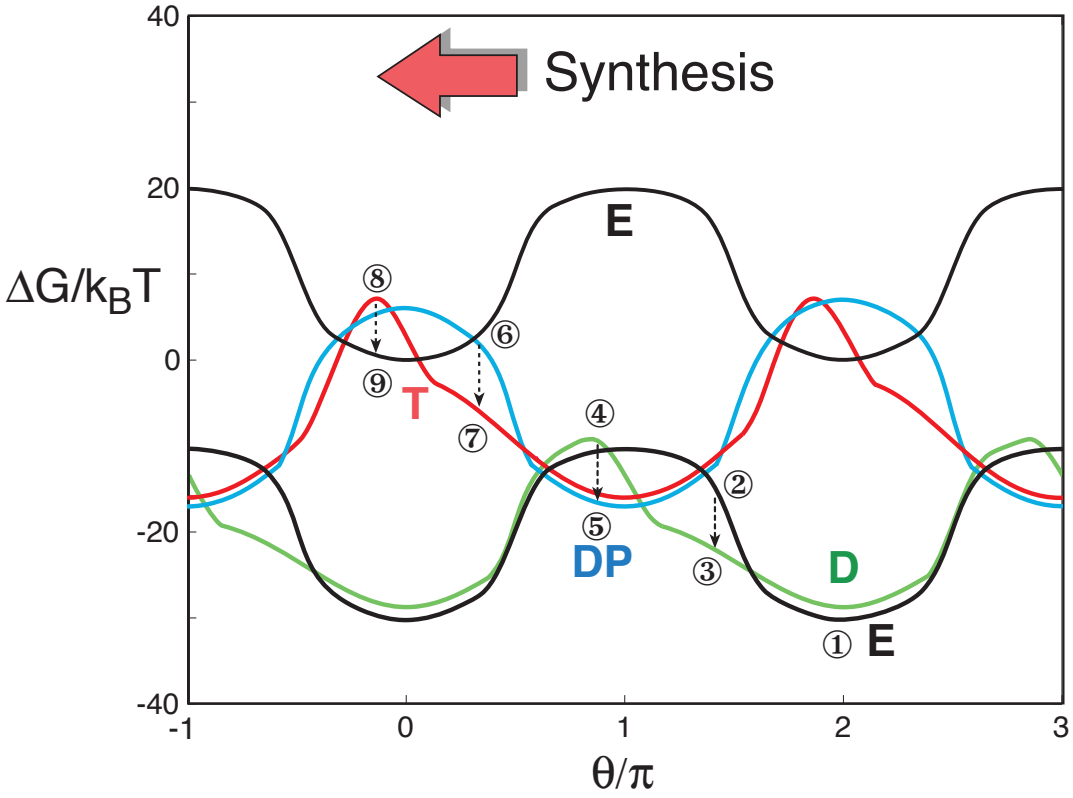

Figure 1. The free energy potentials required for nucleotide synthesis. In a typical cycle starting in the empty state, **E**, at **(1)**, torque from F_o rotates γ to the left. This strains the empty catalytic site, raising its elastic energy. At some point **(2)**, the system drops to point **(3)** on the **D** curve when ADP binds to the site. Further rotation drives the system up the **D** curve until, at point **(4)** phosphate is bound and the system drops to the **DP** potential curve at point **(5)**. Continued rotation further strains the occupied catalytic site driving the system up the **DP** curve until at some point **(6)** ATP is formed at the transition from **(6)** to **(7)**. The system is now trapped in the **T** state where ATP is bound tightly. Rotational torque from F_o must now pry open the active site by straining the system from **(7)** to **(8)** whereupon the nucleotide is released and the system drops to point **(9)** in the empty, **E**, state. The 'bumps' on the elastic energy curves are necessary in order to trap reactants as γ turns to avoid futile rotations. These features can be incorporated into the mechanical model as additional elastic elements. This does not address their origin within the structure of F_1 since there is no unique

relationship between the elastic potentials and a mechanical realization. However, there are certain features of F_1 that are candidate structures. Most noticeably, the ε subunit—which is absent in the hydrolysis experiments (Noji, et al., 1997; Yasuda, et al., 1998)—is in the right position to coordinate the phosphate trap. The ADP and ATP traps also may be ascribed to ε, and/or to strain at the catalytic sites induced by additional elastic elements in β. Specific assignment of these features awaits more detailed structural analysis of F_1.

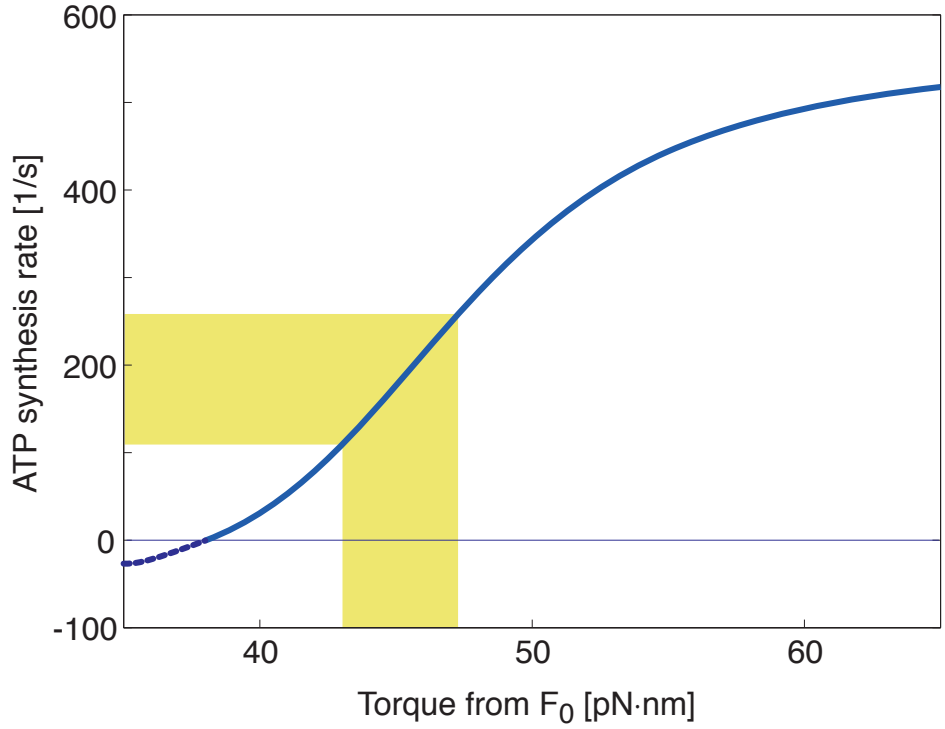

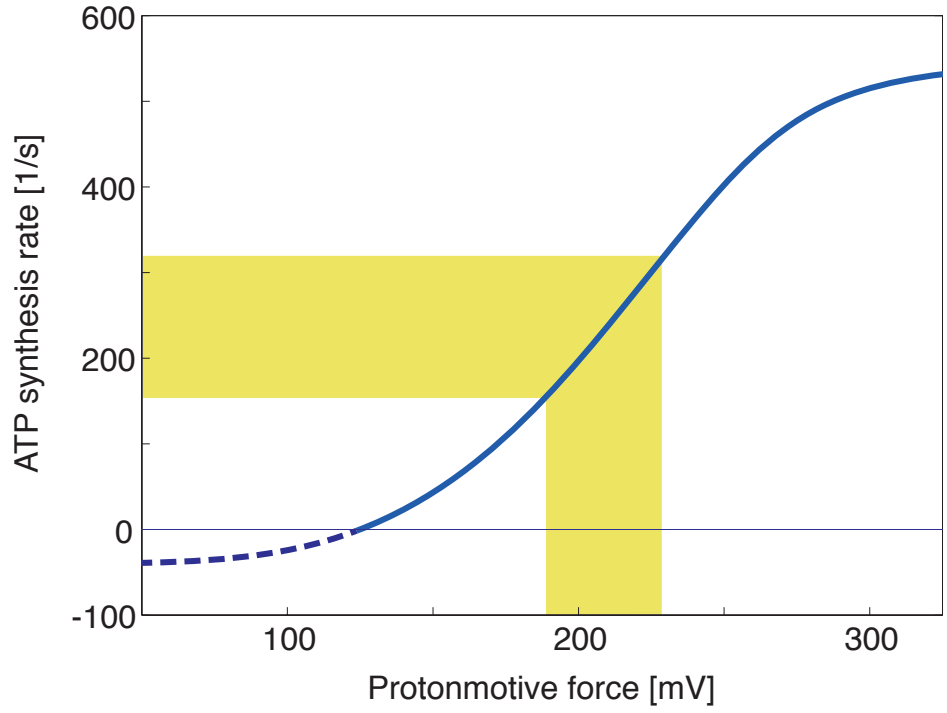

Figure 2. (a) The ATP synthesis rate as a function of the torque applied to the γ shaft. The model predicts the correct synthesis rate when a torque of ~ 45 pN-nm is applied to F_1 (shaded region).

(b) The ATP synthesis rate as a function of the protonmotive force (pmf) imposed across the membrane-spanning F_o subunit. The F_1F_0 complex is modeled by combining the F_1 model in this study with the F_0 model in our previous study (Elston, et al., 1998). When the F_1 and F_0 models are constrained to rotate at the same rate, the model predicts the correct synthesis rate for physiological protonmotive forces (shaded region). The protonmotive force is given by pmf = $\Delta\psi + RT/F\ \Delta pH$, where $\Delta\psi$ is the transmembrane potential, R is the gas constant and F is Faraday's constant. In both (a) and (b), the nucleotide concentrations are [ATP] = 0.2 mM, [ADP] = 0.1 mM and $[P_i]$ = 2 mM. In the experiments of Matsuno-Yagi, this set of concentrations corresponds to the half maximum synthesis rate (Matsuno-Yagi, et al., 1986).

The occupancy of the catalytic sites as a function of ATP concentration

By inserting a tryptophan residue in position β331 of *E. coli* F_1-ATPase, Senior's group designed an optical probe which directly monitors occupancy of the three catalytic sites by nucleotides (Weber, et al., 1997). The relation between the ATP concentration and

the occupancy of the catalytic sites was recorded by repeating the experiment over a wide range of ATP concentrations.

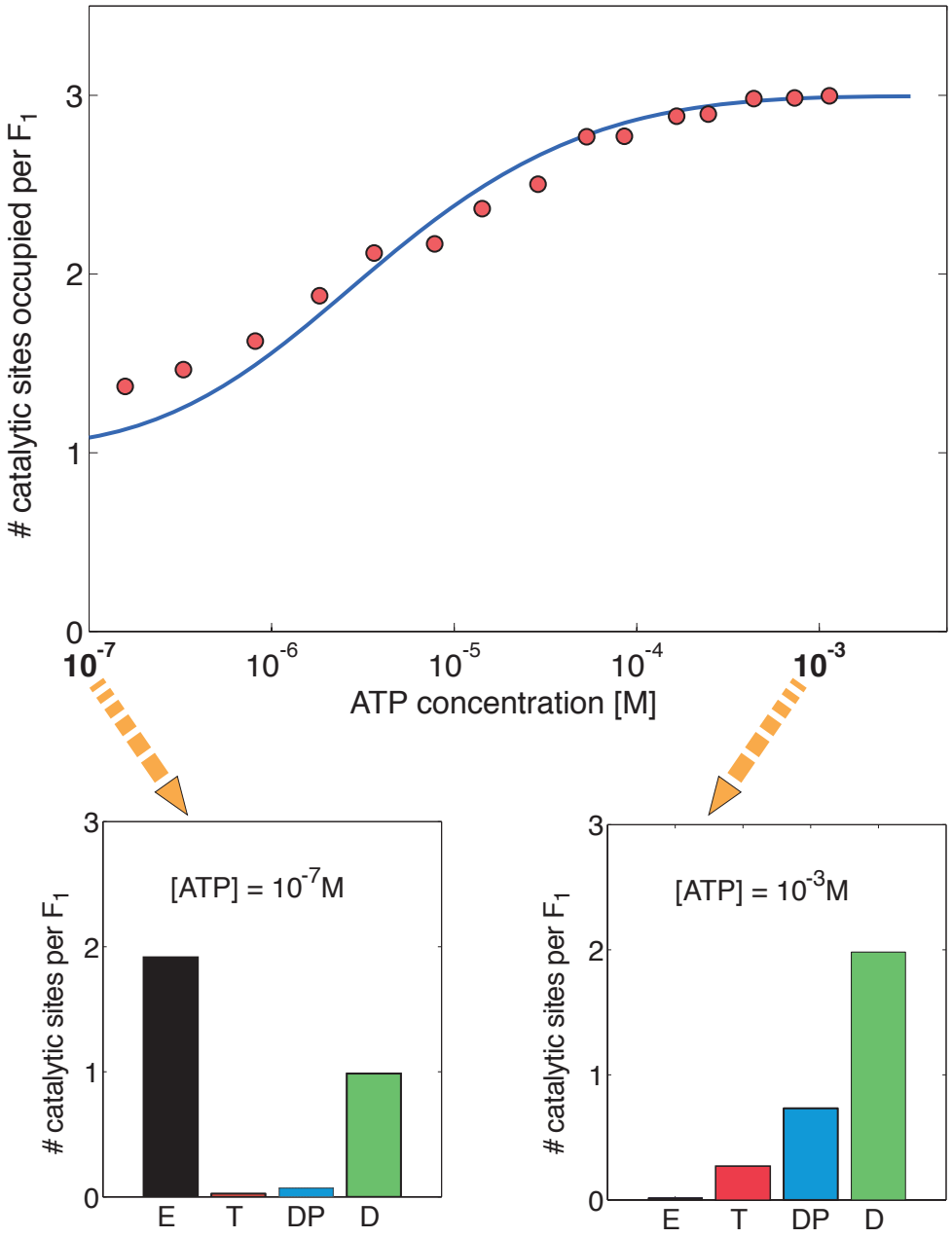

Figure 3. Top panel shows the average number of catalytic sites occupied per F_1 as a function of the ATP concentration. The solid line is the theoretical prediction of the F_1 model and the filled circles are the experimental data from Weber and Senior (Weber, et al., 1997). The two bottom panels show the computed occupancies of the catalytic sites for 10^{-7} M and 10^{-3} M (saturated) ATP concentrations.

As another validity test for the F_1 model, we compared the theoretical prediction of the F_1 model with their experimental results. We calculated the average number of catalytic sites occupied per F_1 as a function of the ATP concentration. In the top panel of Figure 3, the solid line represents the theoretical prediction and the filled circles represent the experimental data from Weber and Senior (Weber, et al., 1997). The F_1 model quantitatively predicts the dependence of the catalytic site occupancy on the ATP concentration. Here a catalytic site in the empty state, **E**, is labeled as unoccupied, otherwise it is labeled as occupied. So an occupied site could be in **T**, **DP** or **D** states. In the two bottom panels of Figure 3, the detailed occupancies of the catalytic sites are computed for low and saturated ATP concentrations.

The proton flux through F_0 coupled to the rotation of γ is blocked by small concentrations of ADP

The F-ATPase couples proton flow to ATP synthesis; in the absence of nucleotide ATP synthesis cannot proceed. However, driven by the torque generated in F_o, the γ shaft can continue to rotate. This rotation of γ allows an unproductive proton flow through the membrane, usually called leakage or proton slip. Groth and Junge found that this proton slip can be blocked by small concentrations of ADP (Groth, et al., 1993). Moreover, in the presence of 0.5 mM P_i, the total proton flow (the sum of the productive and the unproductive proton flows) as a function of the ADP concentration passes through a *minimum*. At low concentrations (less than 1 μM), ADP *reduces* the proton leakage and so the total proton flow decreases with the ADP concentration increases. At concentrations above 1 μM, ADP dramatically *increases* ATP synthesis activity—and the productive proton flux coupled to it—so that the total proton flux increases with the ADP concentration.

We found that the model reproduces this curious experimental observation: proton flux through F_o coupled to the rotation of γ is blocked by small concentrations of ADP, but then increases at the normal synthesis conditions. Figure 4 shows the total proton flux as a function of ADP concentration, predicted by the model. The total proton flux passes through a minimum as the ADP concentration increases from 0.01 μM to 1 mM. P_i concentration is 0.5 mM as in the experiments. This unexpected correlation with experiment supports the assumptions of the model.

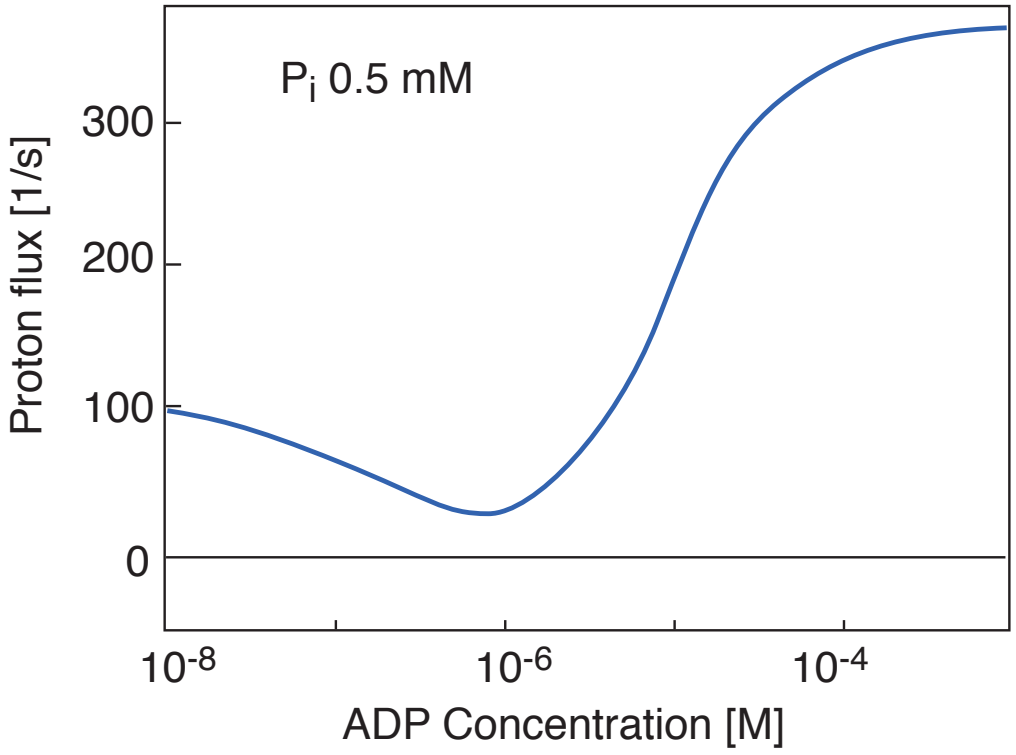

Figure 4. The total proton flux as a function of ADP concentration predicted by the model. The total proton flux passes a minimum as the ADP concentration increases from 0.01 μM to 1 mM (P_I = 0.5 mM). This is in accord with the experimental results in Figure 2a of (Groth, et al., 1993).

Construction of the F_1 motor model

Kinematics and dynamics

Extracting conformational changes from Walker's structure

The molecular structure (PDB) file of F_1-ATPase by Walker's lab (Abrahams, et al., 1994) contains the coordinates of three α's, three β's and part of γ. This file was used to extract approximate conformational changes of each subunit. Figure 5a,b shows a side and top view of F_1 in ribbon display mode; Figure 5c shows a side view in spacefill display mode, and Figure 5d shows a side view of one α, one β and γ in spacefill display mode. The $\alpha_3\beta_3$ hexamer forms an annulus around the γ subunit. There are six ATP binding sites located at the α-β interfaces; the 3 catalytic sites are mostly on the β subunit, while the noncatalytic sites are mostly on the α subunit.

In the experiments of Noji, et. al (Noji, et al., 1997), (Yasuda, et al., 1997) the γ subunit rotates with respect to the $\alpha_3\beta_3$ hexamer as F_1 hydrolyzes ATP. The bottom portion (in Figure 5) of the $\alpha_3\beta_3$ hexamer is symmetric and is thought to constitute the hydrophobic 'bearing' surface between $\alpha_3\beta_3$ and γ. This portion does not change appreciably during the rotation of γ. The γ subunit and the top portion of the $\alpha_3\beta_3$ hexamer are asymmetric and complementary, so that the asymmetry of the γ subunit fits the asymmetry of the hexamer, suggesting that the γ subunit is rotated by changing the asymmetry of the top $\alpha_3\beta_3$ hexamer.

In order to analyze the motions of F_1 we first place a cylindrical coordinate system on the bottom portion of the $\alpha_3\beta_3$ hexamer, since it undergoes little or no conformational change during the rotation of γ. Figure 6a shows a view from the bottom of the barrel portion of F_1 where the symmetry of the $\alpha_3\beta_3$ hexamer is apparent. Three α–carbons from three β-Glu26 residue groups (one from each β) are shown as black dots. These three atoms form an equilateral triangle. We position the origin of our cylindrical coordinate system at the center of this triangle and erect the z-axis perpendicular to the plane of the triangle (pointing from F_1 towards F_o as shown in Figure 6a). We number the β's in the positive rotation direction around the z-axis (clockwise in Figure 6a). Figure 6b is a perspective view of the bottom barrel portion of F_1 with the z-axis pointing upwards.

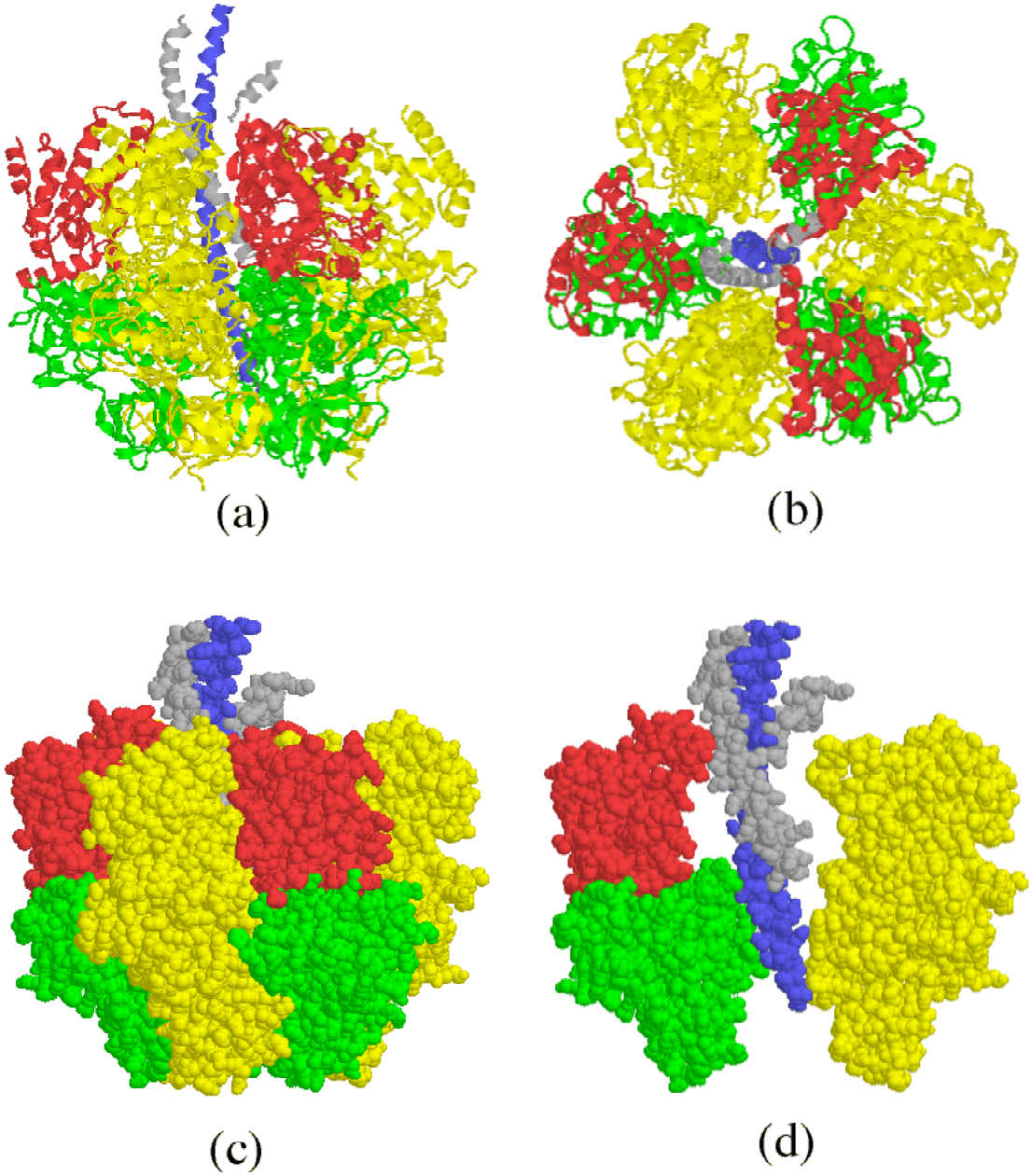

Figure 5 Geometry of F_1. The top row shows a ribbon view from the side (a) and top (b). (c) is a solid (spacefill) view from the side. (d) is a solid view from side of one α, one β and γ. The α's are in yellow; the stationary lower portions of the β's are in green and the moveable upper portions are in red. The two coils of γ are shown in blue and gray. The corresponding animation movies are (a) F1_side.mpeg, (b) F1_top.mpeg, (c) F1_side_fill.mpeg, (d) F1_abg_fill.mpeg.

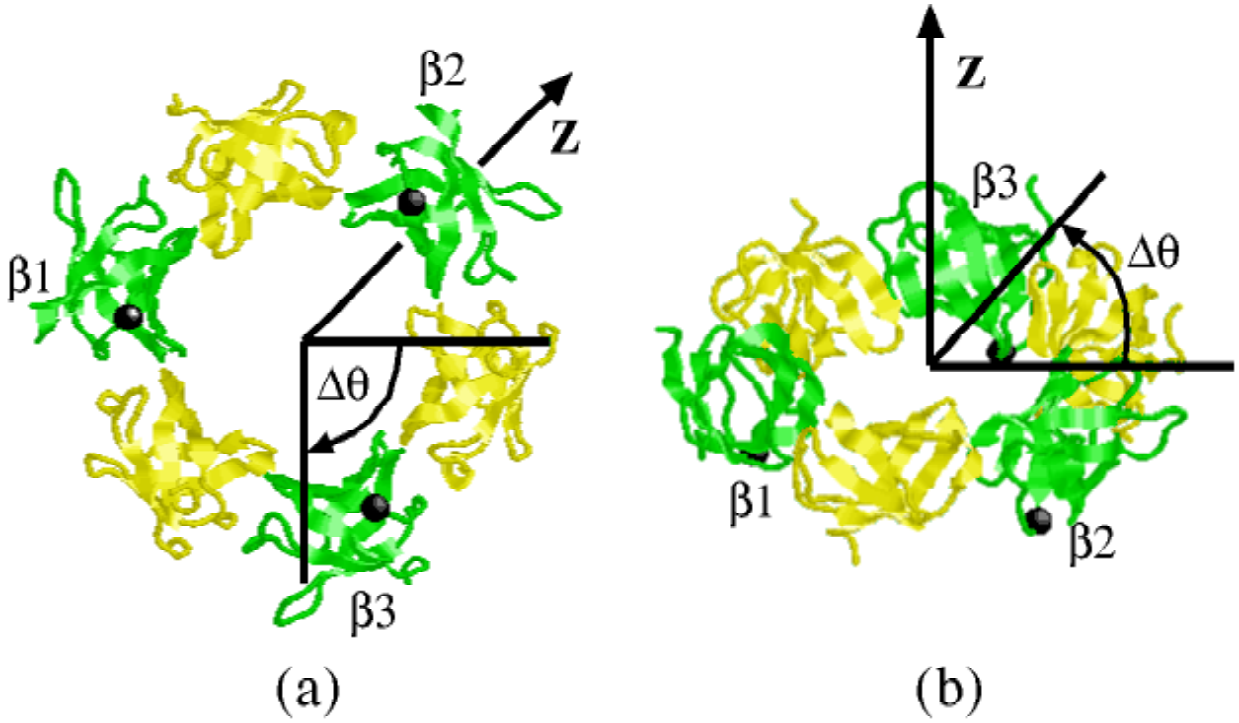

Figure 6 Bottom view (a) and perspective view (b) of the bottom barrel portion of F_1. The three black dots show three α–carbons from three β-Glu26 residues, one from each β. The coordinate system is determined by these three atoms (see text). The color scheme is the same as in Figure 5: α's in yellow, β's in green.

Next we determine the coordinates of each β and α subunit after the γ subunit rotates one third of a revolution. According to Boyer's binding change mechanism (Boyer, 1993), a $2\pi/3$ rotation of the γ subunit corresponds to a $2\pi/3$ advance of the chemical states of the three catalytic sites and a $2\pi/3$ advance of the conformational asymmetry of the $\alpha_3\beta_3$ hexamer. That is, after a $2\pi/3$ rotation of the γ subunit, β_1 takes the configuration of β_3 which is $2\pi/3$ behind β_1, β_2 takes the configuration of β_1 and β_3 takes the configuration of β_2 so that the conformational asymmetry of the $\alpha_3\beta_3$ hexamer propagates by $2\pi/3$. Thus after the γ subunit rotates by $2\pi/3$, the new coordinates of β_1 are the original coordinates of β_3 rotated by $2\pi/3$ in the cylindrical coordinate system. The new coordinates of β_2 and β_3 are calculated from the original coordinates of β_1 and β_2 respectively. The new coordinates of β_1 after a $4\pi/3$ rotation of γ are calculated by rotating the original coordinates of β_2 which is $4\pi/3$ behind β_1. After a 2π rotation of γ, β_1 assumes its original coordinates. For angular displacements of γ between 0 and $2\pi/3$, we estimate the new coordinates of β_1 as a linear interpolation of the coordinates for $\theta=0$ and the coordinates for $\theta=2\pi/3$ in the cylindrical coordinate system. The new coordinates of β_2, β_3, α_1, α_2 and α_3 are calculated accordingly. In this way, we can compute a sequence of configurations corresponding to different angular displacements of γin F_1.

Kinematics of the F_1 motor

Once we knows how to compute the configuration of F_1 for any angular displacement of γ, we can examine the kinematics of the F_1 motor by comparing the configurations of F_1 for different angular displacements of γ. Figure 7 shows four configurations of one α, one β and γ corresponding to angular displacements of γ of $\theta = (0, \pi/4, \pi/2, \pi)$. For clarity, we show only one α, one β and γ, giving a cross sectional view of the $\alpha_3\beta_3$ hexamer. As before, the top portion of the β subunits are colored red and the bottom portion colored green.

From studies such as Figure 7, we can draw the following conclusions about the conformational motions of F_1:

- During the rotation of γ, there is very little conformational change in the bottom portion of the $\alpha_3\beta_3$ hexamer.

- The bottom portion of the $\alpha_3\beta_3$ hexamer forms a symmetric bearing. In Figure 7, the bearing section contained between the middle and bottom rings. Note that both the middle ring and the bottom ring are centered on the z-axis of the coordinate system defined in Figure 6, and they remain unchanged during the rotation of γ.

- The bottom part of the γ subunit fits into the middle and bottom rings. The γ subunit is asymmetric, and the top part of the γ is off the z-axis.

- The top ring is formed by the tips of the $\alpha_3\beta_3$ hexamer which surrounds the top part of γ. This ring is also off the z-axis. The position of this top ring relative to the z-axis determines the position of the top part of γ relative to the z-axis. Since the bottom part of γ is held by two rings centered on the z-axis, the position of the top part of γ relative to the z-axis determines the angular displacement of γ.

From these observations we conclude that the γ subunit is driven by rotation of the off-axis top ring about the centerline, while the middle and bottom rings centered on the z-axis act as bearings for the lower portion of γ. Thus the asymmetrically curved γ subunit is driven by the three β subunits in a fashion analogous to 3 arms cranking an automobile jack. To visualize the motion of F_1, we have used the interpolation program to make movies of F_1 as γ rotates. These movies in MPEG and QuickTime formats can be downloaded from the web site http://teddy.berkeley.edu:1024/ATP_synthase/.

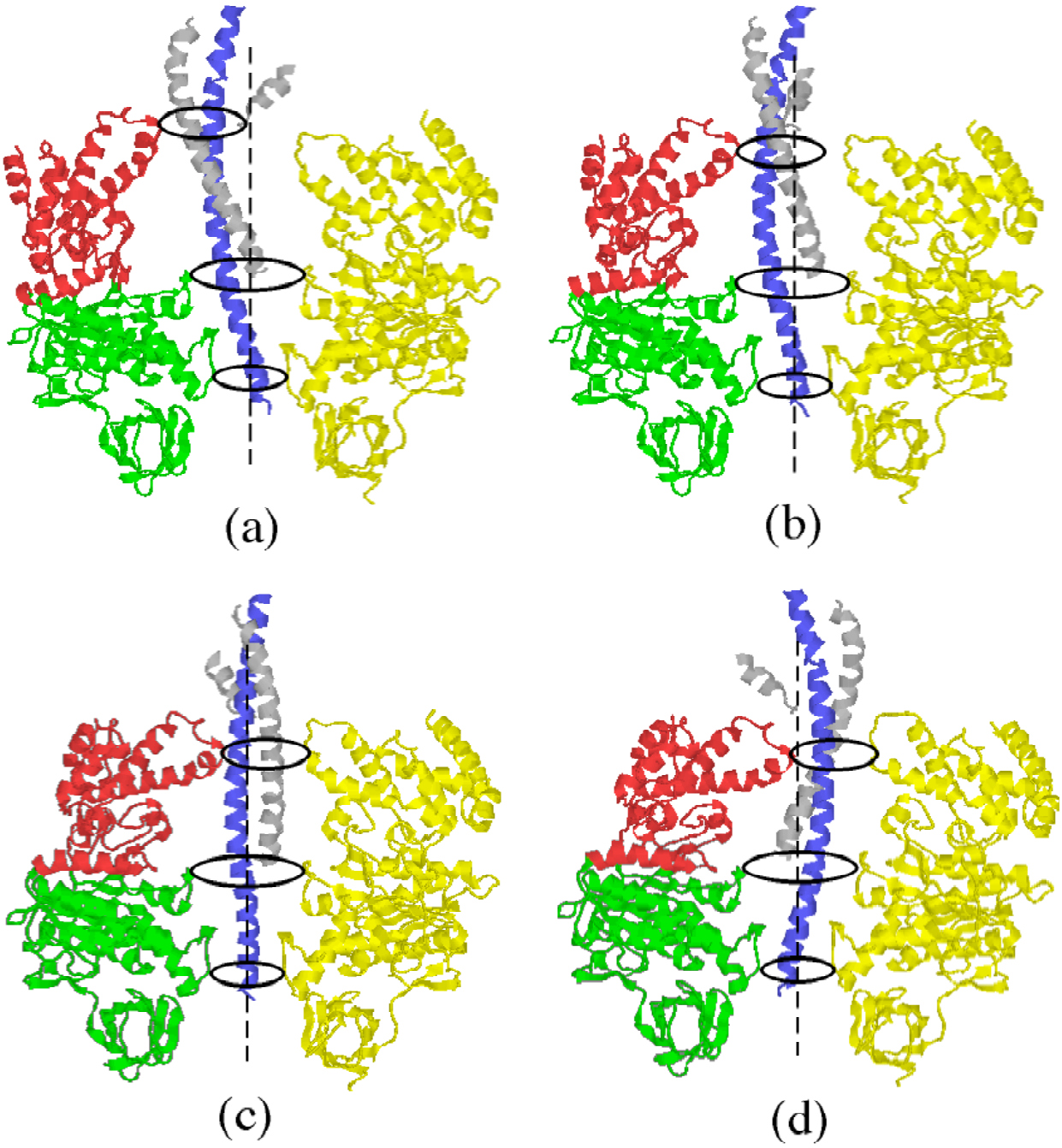

Figure 7 Configurations of one α, one β and γ for several angular displacements of γ: (a) $\theta = 0$, (b) $\theta = \pi/4$, (c) $\theta = \pi/2$, (d) $\theta = \pi$. The circles show the regions of close contact between γ and the annulus in $\alpha_3\beta_3$. The bottom two contact circles remain approximately concentric, while the top contact circle rotates off-center about the vertical axis (dashed line). The corresponding animation movie is F1_abg.mpeg.

F1_3d.mpeg	Perspective view of $\alpha_3\beta_3$ and γ in cartoon display mode.
F1_3d_fill_spc.mpeg	Perspective view of $\alpha_3\beta_3$ and γ in spacefill display mode with specular highlights.
F1_top.mpeg	Top view of $\alpha_3\beta_3$ and γ in cartoon display mode.
F1_top_fill_spc.mpeg	Top view of $\alpha_3\beta_3$ and γ in spacefill display mode with specular highlights.
F1_side.mpeg	Side view of $\alpha_3\beta_3$ and γ in cartoon display mode.
F1_side_fill_spc.mpeg	Side view of $\alpha_3\beta_3$ and γ in spacefill display mode with specular highlights.
F1_abg.mpeg	Cross-section view of one α, one β and γin cartoon display mode.
F1_abg_fill.mpeg	Cross-section view of one α, one β and γin spacefill display mode.
F1_beta.mpeg	Cross-section view of β in cartoon display mode.
F1_beta_fill.mpeg	Cross-section view of β in spacefill display mode.
F1_beta_site.mpeg	A zoom-in view of β near the catalytic site in cartoon display mode.
F1_beta_top.mpeg	Top view of β in cartoon display mode.
F1_alpha.mpeg	Cross-section view of α in cartoon display mode.
F1_Model.mpeg	Animation based on our mechanical model.

Table 1. Index of movies showing the motions of F_1.

Dynamics of the F_1 motor

As shown in Figure 7, the γ subunit is constrained by two rings at the middle and the bottom levels. When the top ring moves around the z-axis, the γ subunit must rotate to accommodate all three rings. That is, the motion of the top ring around the z-axis drives the rotation of the γ subunit. The motion of the top ring is driven, in turn, by hinge motions of each β subunit.

The structure of an empty βsubunit suggests the 'open' configuration is the relaxed state of the empty β subunits (Shirakihara, et al., 1997). The model assumes that the

hinge motion of a β subunit from 'open' to 'closed' is driven by the binding of nucleotide to the catalytic site. We call this introduction of binding free energy at the catalytic site the primary power stroke. It can be modeled as an elastic element which is switched on (stretched and engaged) upon ATP binding at the catalytic site. We shall call this elastic element the 'active spring'.

We further assume that the hinge motion of a β subunit from 'closed' back to 'open' is driven by the 'recoil' elasticity resulting from the compression of the primary power stroke. That is, the secondary power stroke can be modeled by a spring that is compressed during the hinge motion from 'open' to 'closed' of the primary power stroke. This spring represents the intrinsic elasticity of the β subunits, which is established during the initial assembly of the $\alpha_3\beta_3$ hexamer. For this reason, we call this the 'passive spring'. Thus at the completion of the primary power stroke the active spring is switched off, and the β subunit can recoil back to the 'open' configuration driven by the passive spring. This mechanical model captures the essential energy transfers that take place within F_1 during the hydrolysis cycle. The timing and sequence of the energy transfers are controlled by the chemistry of the hydrolysis cycle, which we now discuss.

Kinetics

During ATP synthesis and hydrolysis, each β subunit passes through at least four chemical states (Equation 1 in the text):

$$\underset{\text{Empty}}{\mathbf{E}} \xleftrightarrow{\text{ATP binding}} \underset{\text{ATP bound}}{\mathbf{T}} \xleftrightarrow{\text{Hydrolysis}} \underset{\text{ADP \& } P_i \text{ bound}}{\mathbf{D\cdot P}} \xleftrightarrow{P_i \text{ release}} \underset{\text{ADP bound}}{\mathbf{D}} \xleftrightarrow{\text{ADP release}} \underset{\text{Empty}}{\mathbf{E}} \qquad (1)$$

We denote by $\boldsymbol{\beta_i}$ the chemical state of the ith β subunit, and denote by $\mathbf{S} = (\boldsymbol{\beta_1}, \boldsymbol{\beta_2}, \boldsymbol{\beta_3})$ the chemical state of the $\alpha_3\beta_3$ system. For each β subunit, the possible chemical states are

$$\{\, \mathbf{E, T, D\cdot P, D} \,\}. \qquad (2)$$

The space of the possible kinetic states for the $\alpha_3\beta_3$ system is:

$$\{\, \mathbf{E, T, D\cdot P, D} \,\} \times \{\, \mathbf{E, T, D\cdot P, D} \,\} \times \{\, \mathbf{E, T, D\cdot P, D} \,\}. \qquad (3)$$

These $4^3 = 64$ possible kinetic states can be visualized as the integer points in a 4x4x4 cube. Actually the kinetic states form a 3-dimensional torus, since when the system exits one face of the cube, it reenters the opposite face.

The reaction process at each β catalytic site can be described by the Markov process:

$$\begin{array}{ccc} \mathbf{E} & \longleftrightarrow & \mathbf{T} \\ \updownarrow & & \updownarrow \\ \mathbf{D} & \longleftrightarrow & \mathbf{D \cdot P} \end{array} \tag{4}$$

It is important to stress that the progression of the system through the 64-state cube is stochastic. That is, we do not impose a deterministic sequence of chemical states; we shall specify only the transition rates between states, and let the system evolve stochastically as the dynamics dictates. Thus the formulation given here differs fundamentally from other kinetic schemes proposed for ATP synthase. However, under some circumstances (e.g. ambient concentrations), there may be a most probable path. We formulate the stochastic dynamics of the three catalytic sites as follows.

Let $\rho(\theta; t, \beta_{i-1}, \beta_\upsilon, \beta_{i+1})$ be the probability at time t that the β's are in chemical states $\boldsymbol{\beta}_{i-1}$, $\boldsymbol{\beta}_i$ and $\boldsymbol{\beta}_{i+1}$, respectively, while γ is fixed at an angular position θ. Note that $\rho(\theta; t, \beta_{i-1}, \beta_\upsilon, \beta_{i+1})$ is NOT the probability density that γ is at the angular position θ at time t, and the β's are in chemical states $\boldsymbol{\beta}_{i-1}$, $\boldsymbol{\beta}_i$ and $\boldsymbol{\beta}_{i+1}$, respectively. Here θ is a parameter. By fixing the γ subunit at an angular position, we are able to isolate the kinetics and study its governing equation. In the subsequent sections, we will combine the kinetics and the dynamics to build a complete model for F_1 motor.

The governing equation for the Markov process on β_i is

$$\frac{d}{dt}\begin{bmatrix} \rho(\theta; t, \beta_{i-1}, E, \beta_{i+1}) \\ \rho(\theta; t, \beta_{i-1}, T, \beta_{i+1}) \\ \rho(\theta; t, \beta_{i-1}, DP, \beta_{i+1}) \\ \rho(\theta; t, \beta_{i-1}, D, \beta_{i+1}) \end{bmatrix} = \begin{bmatrix} -\Sigma_E & k_{T\to E} & 0 & k_{D\to E} \\ k_{E\to T} & -\Sigma_T & k_{DP\to T} & 0 \\ 0 & k_{T\to DP} & -\Sigma_{DP} & k_{D\to DP} \\ k_{E\to D} & 0 & k_{DP\to D} & -\Sigma_D \end{bmatrix} \cdot \begin{bmatrix} \rho(\theta; t, \beta_{i-1}, E, \beta_{i+1}) \\ \rho(\theta; t, \beta_{i-1}, T, \beta_{i+1}) \\ \rho(\theta; t, \beta_{i-1}, DP, \beta_{i+1}) \\ \rho(\theta; t, \beta_{i-1}, D, \beta_{i+1}) \end{bmatrix} \tag{5}$$

where

$$\begin{aligned} \Sigma_E &= k_{E\to T} + k_{E\to D} \\ \Sigma_T &= k_{T\to E} + k_{T\to DP} \\ \Sigma_{DP} &= k_{DP\to T} + k_{DP\to D} \\ \Sigma_D &= k_{D\to E} + k_{D\to DP} \end{aligned} \tag{6}$$

All transition rates depend on θ, the angular position of γ relative to β, and the chemical states of the other two β's:

$$\begin{aligned} k_{E\to T} &= k_{E\to T}(\theta, \beta_{i-1}, \beta_{i+1}), \\ k_{T\to DP} &= k_{T\to DP}(\theta, \beta_{i-1}, \beta_{i+1}), \\ &\cdots \end{aligned} \tag{7}$$

In the matrix-vector form, equation (5) is

$$\frac{d}{dt}\rho_i(\theta; t, \beta_{i-1}, \beta_{i+1}) = \mathbf{K}(\theta, \beta_{i-1}, \beta_{i+1}) \cdot \rho_i(\theta; t, \beta_{i-1}, \beta_{i+1}) \tag{8}$$

where

$$\rho_i(\theta; t, \beta_{i-1}, \beta_{i+1}) = \begin{bmatrix} \rho(\theta; t, \beta_{i-1}, E, \beta_{i+1}) \\ \rho(\theta; t, \beta_{i-1}, T, \beta_{i+1}) \\ \rho(\theta; t, \beta_{i-1}, DP, \beta_{i+1}) \\ \rho(\theta; t, \beta_{i-1}, D, \beta_{i+1}) \end{bmatrix} \tag{9}$$

In Equation 2 in the text, we write equation (8) symbolically as:

$$\frac{d\beta_i}{dt} = \mathbf{K}(\theta, \beta_{i-1}, \beta_{i+1}) \cdot \beta_i \quad , \qquad i = 1,2,3 \tag{10}$$

There are 16 choices for the combination of (β_{i-1}, β_{i+1}). So there are 16 different probability density vector, ρ_i, each of which is a vector with 4 components. These ρ_i's form a vector with 64 elements.

$$\boldsymbol{\rho}(\theta; t) = \left.\begin{bmatrix} \rho(\theta; t, E, E, E) \\ \rho(\theta; t, E, E, T) \\ \rho(\theta; t, E, E, DP) \\ \rho(\theta; t, E, E, D) \\ \rho(\theta; t, E, T, E) \\ \vdots \\ \rho(\theta; t, D, D, DP) \\ \rho(\theta; t, D, D, D) \end{bmatrix}\right\} 64 \text{ components} \tag{11}$$

Combining equation (5) for all combinations of (β_{i-1}, β_{i+1}), we have the governing equation for the probability vector, $\rho(\theta, t)$, of the $\alpha_3\beta_3$ system:

$$\frac{d}{dt}\boldsymbol{\rho}(\theta; t) = \mathbf{K}(\theta) \cdot \boldsymbol{\rho}(\theta; t) \tag{12}$$

where the transition matrix $\mathbf{K}(\theta)$ is a 64x64 sparse matrix with only 6x64=384 non-zero elements. The elements of the transition matrix of the system, $\mathbf{K}(\theta)$, are related to the elements of the transition matrix of the ith β, $\mathbf{K}(\theta, \beta_{i-1}, \beta_{i+1})$, as:

$$
\begin{aligned}
k_{(E,E,E)\to(E,T,E)}(\theta) &= k_{E\to T}(\theta, E, E),\\
k_{(E,E,E)\to(E,E,T)}(\theta) &= k_{E\to T}\left(\theta - \frac{2\pi}{3}, E, E\right),\\
k_{(E,E,E)\to(T,E,E)}(\theta) &= k_{E\to T}\left(\theta + \frac{2\pi}{3}, E, E\right),\\
&\cdots
\end{aligned}
\tag{13}
$$

Hence we only need to consider the transition matrix of one β for 16 different chemical state combinations of the other two β's.

Coupling of the reaction on β to the rotation of γ

To simulate the chemical reactions taking place at each catalytic site, we must construct the transition matrix of one β for 16 different chemical state combinations at the other two β's. Since each transition matrix has 8 non-zero elements (see equation (5)), there are 8×16 independent transition rates. However, we can build all of these starting from the uni-site reaction rates listed in Table 2 (Senior, 1992).

The multisite reaction rates are affected by several factors:

1. The chemical states of the other two sites, β_{i-1} and β_{i+1},
2. The positions of switches S1 and S2 on γ relative to β (θ dependence),
3. The elastic energy difference between the two chemical states of the β under consideration (θ dependent).

The word 'multisite' suggests that factor #1 is most important; however, the fast multisite reactions are only observed when more than one catalytic site is occupied and the γ subunit is present (Kaibara, et al., 1996). This implies that the γ subunit plays an important role in the multisite reactions, and so factors #2 and #3 must be taken into consideration.

We can express these factors mathematically as:

$$
\begin{aligned}
k^{M}_{forward}(\theta, \beta_{i-1}, \beta_{i+1}) &= k^{U}_{forward} \cdot f(\beta_{i-1}, \beta_{i+1}) \cdot g(\theta) \cdot \exp\left(\frac{\lambda \cdot \Delta E(\theta)}{k_B T}\right)\\
k^{M}_{backward}(\theta, \beta_{i-1}, \beta_{i+1}) &= k^{U}_{backward} \cdot f(\beta_{i-1}, \beta_{i+1}) \cdot g(\theta) \cdot \exp\left(\frac{-(1-\lambda) \cdot \Delta E(\theta)}{k_B T}\right)
\end{aligned}
\tag{14}
$$

where k^M represents the multisite transition rates between two chemical states, k^U represents the unisite rates. The function $f(\beta_{i-1}, \beta_{i+1})$ represents the effect of the other two sites, $g(\theta)$ simulates the effect of the two switches on γ, and $\Delta E(\theta)$ is the elastic energy difference between the two chemical states of the β under consideration. To

keep the notation simple, we shall drop the superscript M for multisite rates from now on.

Table 2 summarizes the mathematical formulation of the multisite reaction rates along with the unisite rates and other parameter values.

PARAMETERS	VALUES
Unisite reaction rates of *E. Coli.* (Senior, 1992)	$k^U_{E\to T} = 1.1\times10^5\ s^{-1}\ M^{-1}$, $k^U_{T\to E} = 2.5\times10^{-5}\ s^{-1}$ $k^U_{T\to DP} = 1.2\times10^{-1}\ s^{-1}$, $k^U_{DP\to T} = 4.3\times10^{-2}\ s^{-1}$ $k^U_{DP\to D} = 1.2\times10^{-3}\ s^{-1}$, $k^U_{D\to DP} = 4.8\times10^{-4}\ s^{-1}\ M^{-1}$ $k^U_{D\to E} = 1.6\times10^{-3}\ s^{-1}$, $k^U_{E\to D} = 1.8\times10^{2}\ s^{-1}\ M^{-1}$
Free energy drops of unisite reaction of *E. Coli.*	$\Delta G_{E\to T} = \Delta G^0_{E\to T} + \log([ATP]/M)\cdot k_BT$ $\Delta G^0_{E\to T} = \log(k^U_{E\to T} / k^U_{T\to E}) = 22.2\ k_BT$ $\Delta G_{T\to DP} = \log(k^U_{T\to DP} / k^U_{DP\to T}) = 1.0\ k_BT$ $\Delta G_{DP\to D} = \Delta G^0_{DP\to D} - \log([Pi]/M)\cdot k_BT$ $\Delta G^0_{DP\to D} = \log(k^U_{DP\to D} / k^U_{D\to DP}) = 0.9\ k_BT$ $\Delta G_{D\to E} = \Delta G^0_{D\to E} - \log([ADP]/M)\cdot k_BT$ $\Delta G^0_{D\to E} = \log(k^U_{D\to E} / k^U_{E\to D}) = -11.6\ k_BT$

PARAMETERS	VALUES
Construction of the multisite reaction rate, k^M, from the unisite rate, k^U.	$k^M_{forward}(\theta, \beta_{i-1}, \beta_{i+1}) = k^U_{forward} \cdot f(\beta_{i-1}, \beta_{i+1}) \cdot g(\theta) \cdot \exp\left(\frac{\lambda \cdot \Delta E(\theta)}{k_B T}\right)$ $k^M_{backward}(\theta, \beta_{i-1}, \beta_{i+1}) = k^U_{backward} \cdot f(\beta_{i-1}, \beta_{i+1}) \cdot g(\theta) \cdot \exp\left(\frac{-(1-\lambda) \cdot \Delta E(\theta)}{k_B T}\right)$ $f(\beta_{i-1}, \beta_{i+1})$ simulates the effect of the occupancy of the other two sites (i.e. binding of ATP on other sites increases the reaction on this site). $g(\theta)$ simulates the effect of the two switches S_1 and S_2 on γ (i.e. rotation of γ brings the switches close to (or away from) this site, which increases (or decreases) the reaction on this site). $\Delta E(\theta)$ is the elastic energy difference between the two chemical states of the β in consideration (θ dependent). See Table 3 for details of the multisite reaction rates.
Elasticity constants of the active and passive springs	$k_{Active} = 10$ pN/nm, $k_{Passive} = 4$ pN/nm The active and passive springs are pre-stretched (pre-compressed) by 4 nm. During the reaction, the additional displacement of these springs is 2 nm.

Table 2. Unisite reaction rates, elasticity constants and the mathematical formulation of the multisite reaction rates.

It should be pointed out that the formulation in equation (14) is a very general one. Once more experimental data are available, more refined models can be accommodated easily into this framework and simulated. Next we discuss the multisite reaction rates in detail.

Transitions between E and T

$$\begin{aligned} k_{E\to T}(\theta, \beta_{i-1}, \beta_{i+1}) &= k^U_{E\to T} \cdot f_{E,T}(\beta_{i-1}, \beta_{i+1}) \cdot g_{E,T}(\theta), \\ k_{T\to E}(\theta, \beta_{i-1}, \beta_{i+1}) &= k^U_{T\to E} \cdot f_{E,T}(\beta_{i-1}, \beta_{i+1}) \cdot g_{E,T}(\theta) \\ &\quad \cdot \exp\left(\frac{(E_T - E_T(\pi)) - (E_E - E_E(0))}{k_B T}\right) \end{aligned} \tag{15}$$

$$f_{E,T}(\beta_{i-1}, \beta_{i+1}) = \begin{cases} 1 & \beta_{i-1} = \beta_{i+1} = E \quad \text{(unisite mode)} \\ 150 & \text{otherwise} \quad \text{(multisite mode)} \end{cases} \tag{16}$$

$$g_{E,T}(\theta) = \begin{cases} 1 & 0 < \theta < \pi/2 \\ & \text{ATP binding promoted by switch \#1} \\ 0.05 & -\pi/2 < \theta < 0 \text{ and one of } (\beta_{i-1}, \beta_{i+1}) \text{ is E} \\ & \text{allows ATP binding on the wrong site} \\ 0 & \text{otherwise} \end{cases} \tag{17}$$

where E_E and E_T are the total elastic energy of the β in state **E** and **T**, respectively.

In equation (16), $f_{E,T}(\beta_{i-1}, \beta_{i+1})$ takes only two values. The effect of the chemical states of the other two sites is modeled as either putting the system into the unisite mode or the multisite mode.

Equation (17) contains both the effect of stress at the catalytic site and the effect of switch #1. The configuration of the catalytic site is related to the angular position, θ, of γ. The site is 'open' near $\theta = 0$ (Figure 7a) and is 'closed' near $\theta = \pi$ (Figure 7d). Since the system is periodic in the θ-direction, $\theta = -\pi$ represents the same angular position as $\theta = \pi$. In equation (17), ATP binding is allowed only when the angular position, θ, is in the region $[-\pi/2, \pi/2]$ where the catalytic site is 'open'. The ATP binding in the θ–range $[0, \pi/2]$ contributes to the forward rotation of the motor while the ATP binding in the θ–range $[-\pi/2, 0]$ leads to a backward step. Switch #1 on the γ subunit promotes ATP binding in the θ–range $[0, \pi/2]$, but does not completely inhibit the ATP binding in the θ–range $[-\pi/2, 0]$. This allows the occasional backward steps.

Transitions between T and D·P

$$\begin{aligned} k_{T\to DP}(\theta, \beta_{i-1}, \beta_{i+1}) &= k^{U}_{T\to DP} \cdot f_{T,DP}(\beta_{i-1}, \beta_{i+1}) \cdot g_{T,DP}(\theta) \cdot \exp\left(\frac{-E^{B}_{DP}}{k_B T}\right) \\ k_{DP\to T}(\theta, \beta_{i-1}, \beta_{i+1}) &= k^{U}_{DP\to T} \cdot f_{T,DP}(\beta_{i-1}, \beta_{i+1}) \cdot g_{T,DP}(\theta) \cdot \exp\left(\frac{-E^{B}_{T}}{k_B T}\right) \end{aligned} \tag{18}$$

$$f_{T,DP}(\beta_{i-1}, \beta_{i+1}) = \begin{cases} 1 & \beta_{i-1} = \beta_{i+1} = E \quad \text{(unisite mode)} \\ 10^5 & \text{otherwise} \quad \text{(multisite mode)} \end{cases} \tag{19}$$

$$g_{T,DP}(\theta) = 1 \tag{20}$$

The total elastic energy of a β consists of three parts:

$$E = E^A + E^P + E^B \tag{21}$$

E^A and E^P are the elastic energies associated with the 'active' and 'passive' springs, respectively, and E^B is the elastic energy associated with the 'bumps' required during synthesis (see below).

The active spring is switched on only in states **T** and **D·P** while the passive spring is always engaged. Thus the total elastic energies of the β for states **E, T, D·P** and **D** are given respectively by

$$\begin{aligned} E_E &= E^P + E^B_E \\ E_T &= E^A + E^P + E^B_T \\ E_{DP} &= E^A + E^P + E^B_{DP} \\ E_D &= E^P + E^B_D \end{aligned} \tag{22}$$

In equation (18), E^B_{DP} is the part of the elastic energy of the β in state D·P that is caused by the additional interaction between the β and the γ, and by the additional elastic components (other than the two major springs) of the β. Correspondingly E^B_T is that part of the elastic energy of the β in state T.

We use superscript 'B' to denote the additional elastic energy associated with the 'bumps' in the elastic energy curves. These bumps are not necessary when F_1 is hydrolyzing ATP and functioning as a motor. However, they are essential when F_1 is turned in the reverse direction by F_o to synthesize ATP. The function of these bumps in ATP synthesis is to prevent 'futile' rotations. When the γ subunit is turned one full revolution in the reverse direction, on average, each β should pass once through the cycle

$$\mathbf{E} \rightarrow \mathbf{D} \rightarrow \mathbf{D \cdot P} \rightarrow \mathbf{T} \rightarrow \mathbf{E} \tag{23}$$

and produce one ATP. Failure of a β to produce an ATP is a futile rotation. Futile rotations can come about in several ways:

1. ADP does not bind on the catalytic site and β stays in state **E.**
2. After binding of ADP, no P_i binds on the catalytic site and β either stays in state **D** or loses its ADP and reverts back to state **E.**

3. After the binding of P_i, ATP does not form and β either stays in state **D·P** or loses its P_I and/or ADP, reverting back to states **D** or **E.**

4. After the formation of ATP from ADP and P_i, ATP is not released from the catalytic site and β either stays in state **T** or reverts back to states **D·P**, **D** or **E.**

To prevent these futile rotations, we need to coordinate sub-steps in the ATP synthesis reaction to the rotation of γ. More specifically, as γ rotates, we guide the β from state **E** into state **D** (ADP binding), then into state **D·P** (Pi binding), then into state **T** (forming ATP from ADP and Pi), and finally back into state **E** again (releasing ATP from the catalytic site).

The important roles of the additional elastic energies (E^B_E, E^B_T, E^B_{DP} and E^B_D) in the ATP synthesis are shown in Figure 1.

Transitions between D·P and D

$$\begin{aligned} k_{DP\to D}(\theta, \beta_{i-1}, \beta_{i+1}) &= k^U_{DP\to D} \cdot f_{DP,D}(\beta_{i-1}, \beta_{i+1}) \cdot g_{DP,D}(\theta) \\ &\quad \cdot \exp\left(\frac{(E_{DP} - E_{DP}(\pi))}{k_B T}\right) \\ k_{D\to DP}(\theta, \beta_{i-1}, \beta_{i+1}) &= k^U_{D\to DP} \cdot f_{DP,D}(\beta_{i-1}, \beta_{i+1}) \cdot g_{DP,D}(\theta) \\ &\quad \cdot \exp\left(\frac{(E_D - E_D(0))}{k_B T}\right) \end{aligned} \tag{24}$$

$$f_{DP,D}(\beta_{i-1}, \beta_{i+1}) = \begin{cases} 1 & \beta_{i-1} = \beta_{i+1} = E \quad \text{(unisite mode)} \\ 10^6 & \text{otherwise} \quad \text{(multisite mode)} \end{cases} \tag{25}$$

$$g_{DP,D}(\theta) = \begin{cases} 1 & \pi < \theta < \dfrac{4\pi}{3} \quad \text{(switch \#2)} \\ 0 & \text{otherwise} \end{cases} \tag{26}$$

In equation (26), Pi release (Pi binding in the ATP synthesis direction) is regulated by switch #2 on the γ subunit.

Transitions between D and E

$$\begin{aligned} k_{D\to E}(\theta, \beta_{i-1}, \beta_{i+1}) &= k^U_{D\to E} \cdot f_{D,E}(\beta_{i-1}, \beta_{i+1}) \cdot g_{D,E}(\theta) \cdot \exp\left(\frac{-E^B_E}{k_B T}\right) \\ k_{E\to D}(\theta, \beta_{i-1}, \beta_{i+1}) &= k^U_{E\to D} \cdot f_{D,E}(\beta_{i-1}, \beta_{i+1}) \cdot g_{D,E}(\theta) \cdot \exp\left(\frac{-E^B_D}{k_B T}\right) \end{aligned} \tag{27}$$

$$f_{D,E}(\beta_{i-1}, \beta_{i+1}) = \begin{cases} 1 & \beta_{i-1} = \beta_{i+1} = E \quad \text{(unisite mode)} \\ 3 \times 10^4 & \text{otherwise} \quad \text{(multisite mode)} \end{cases} \tag{28}$$

$$g_{DP,D}(\theta) = \begin{cases} 1 & -\frac{2\pi}{3} < \theta < \frac{2\pi}{3} \quad \begin{pmatrix} \text{binding regulated by} \\ \text{site configuration} \end{pmatrix} \\ 0 & \text{otherwise} \end{cases} \tag{29}$$

In equation (29), the ADP release (ADP binding in the ATP synthesis direction) is regulated by the configuration of the catalytic site.

PARAMETERS	VALUES
$k_{E\to T}$ and $k_{T\to E}$	$k_{E\to T}(\theta, \beta_{i-1}, \beta_{i+1}) = k^{U}_{E\to T} \cdot f_{E,T}(\beta_{i-1}, \beta_{i+1}) \cdot g_{E,T}(\theta)$, $k_{T\to E}(\theta, \beta_{i-1}, \beta_{i+1}) = k^{U}_{T\to E} \cdot f_{E,T}(\beta_{i-1}, \beta_{i+1}) \cdot g_{E,T}(\theta) \cdot \exp\left(\frac{(E_T - E_T(\pi)) - (E_E - E_E(0))}{k_B T}\right)$ $f_{E,T}(\beta_{i-1}, \beta_{i+1}) = \begin{cases} 1 & \beta_{i-1} = \beta_{i+1} = E \quad \text{(unisite mode)} \\ 150 & \text{otherwise} \quad \text{(multisite mode)} \end{cases}$ $g_{E,T}(\theta) = \begin{cases} 1 & 0 < \theta < \pi/2 \\ & \text{ATP binding promoted by switch \#1} \\ 0.05 & -\pi/2 < \theta < 0 \text{ and one of } (\beta_{i-1}, \beta_{i+1}) \text{ is E} \\ & \text{allows ATP binding on the wrong site} \\ 0 & \text{otherwise} \end{cases}$ E_T is the total elastic energy of the β in state **T.** E_E is the total elastic energy of the β in state **E.**
$k_{T\to DP}$ and $k_{DP\to T}$	$k_{T\to DP}(\theta, \beta_{i-1}, \beta_{i+1}) = k^{U}_{T\to DP} \cdot f_{T,DP}(\beta_{i-1}, \beta_{i+1}) \cdot g_{T,DP}(\theta) \cdot \exp\left(\frac{-E^{B}_{DP}}{k_B T}\right)$ $k_{DP\to T}(\theta, \beta_{i-1}, \beta_{i+1}) = k^{U}_{DP\to T} \cdot f_{T,DP}(\beta_{i-1}, \beta_{i+1}) \cdot g_{T,DP}(\theta) \cdot \exp\left(\frac{-E^{B}_{T}}{k_B T}\right)$ $f_{T,DP}(\beta_{i-1}, \beta_{i+1}) = \begin{cases} 1 & \beta_{i-1} = \beta_{i+1} = E \quad \text{(unisite mode)} \\ 10^5 & \text{otherwise} \quad \text{(multisite mode)} \end{cases}$ $g_{T,DP}(\theta) = 1$ E^{B}_{DP} is the part of the elastic energy of the β in state D·P that is caused by the additional interaction between the β and the γ, and by the additional elastic components (other than the two major springs) of the β.

PARAMETERS	VALUES
$k_{DP\to D}$ and $k_{D\to DP}$	$k_{DP\to D}(\theta, \beta_{i-1}, \beta_{i+1}) = k^{U}_{DP\to D} \cdot f_{DP,D}(\beta_{i-1}, \beta_{i+1}) \cdot g_{DP,D}(\theta) \cdot \exp\left(\frac{(E_{DP} - E_{DP}(\pi))}{k_B T}\right)$ $k_{D\to DP}(\theta, \beta_{i-1}, \beta_{i+1}) = k^{U}_{D\to DP} \cdot f_{DP,D}(\beta_{i-1}, \beta_{i+1}) \cdot g_{DP,D}(\theta) \cdot \exp\left(\frac{(E_{D} - E_{D}(0))}{k_B T}\right)$ $f_{DP,D}(\beta_{i-1}, \beta_{i+1}) = \begin{cases} 1 & \beta_{i-1} = \beta_{i+1} = E \quad \text{(unisite mode)} \\ 10^6 & \text{otherwise} \quad \text{(multisite mode)} \end{cases}$ $g_{DP,D}(\theta) = \begin{cases} 1 & \pi < \theta < \frac{4\pi}{3} \quad \text{(switch \# 2)} \\ 0 & \text{otherwise} \end{cases}$
$k_{D\to E}$ and $k_{E\to D}$	$k_{D\to E}(\theta, \beta_{i-1}, \beta_{i+1}) = k^{U}_{D\to E} \cdot f_{D,E}(\beta_{i-1}, \beta_{i+1}) \cdot g_{D,E}(\theta) \cdot \exp\left(\frac{-E^{B}_{E}}{k_B T}\right)$ $k_{E\to D}(\theta, \beta_{i-1}, \beta_{i+1}) = k^{U}_{E\to D} \cdot f_{D,E}(\beta_{i-1}, \beta_{i+1}) \cdot g_{D,E}(\theta) \cdot \exp\left(\frac{-E^{B}_{D}}{k_B T}\right)$ $f_{D,E}(\beta_{i-1}, \beta_{i+1}) = \begin{cases} 1 & \beta_{i-1} = \beta_{i+1} = E \quad \text{(unisite mode)} \\ 3\times 10^4 & \text{otherwise} \quad \text{(multisite mode)} \end{cases}$ $g_{DP,D}(\theta) = \begin{cases} 1 & -\frac{2\pi}{3} < \theta < \frac{2\pi}{3} \quad \begin{pmatrix}\text{binding regulated by} \\ \text{site configuration}\end{pmatrix} \\ 0 & \text{otherwise} \end{cases}$ E^{B}_{D} is the part of the elastic energy of the β in state D that is caused by the additional interaction between the β and the γ, and by the additional elastic components (other than the two major springs) of the β.

Table 3. Multisite reaction rates

Calculating the elastic potentials

Figure 8 shows how the bending angle, ϕ, of the β subunit is coupled to the rotational angle, θ, of the γ subunit. In the left panel, the plane shown is perpendicular to the rotation axis of γ. The dashed circle represents the cross-section of γ at the hydrophobic 'bearing' section where the γ is held tightly at two levels (middle and bottom levels in Figure 7). The solid filled circle represents the cross section of the γ at the 'driving' level where γ contacts the bending β subunits. The three small filled circles represent the three hinge points on the three β's. The solid lines between the hinge points and the γ are the projection of the top parts of the β's onto the plane perpendicular to the γaxis. L(θ) is the length of the top part of each β projected onto the plane perpendicular to the γ axis; it is a function of the rotation angle, θ, of γ. In the right panel, the plane shown is parallel to the γ axis. The top and bottom sectors of β are shown schematically as line segments. The dashed line represents the relaxed position of the top sector of an empty β. The azimuthal angle between the top and bottom sectors, ϕ, measures the bending angle of β. L(ϕ) is the length of the top part of β projected onto the plane perpendicular to the γ axis; it is a function of the bending angle, ϕ. By equating L(θ) and L(ϕ), we obtain a relation between the bending angle, ϕ, and the rotational angle, θ. If we assume the active and passive springs connecting the top and bottom parts of each β are linear in the bending angle, ϕ, we can calculate the potential caused by these two springs as a function of the rotational angle, θ.

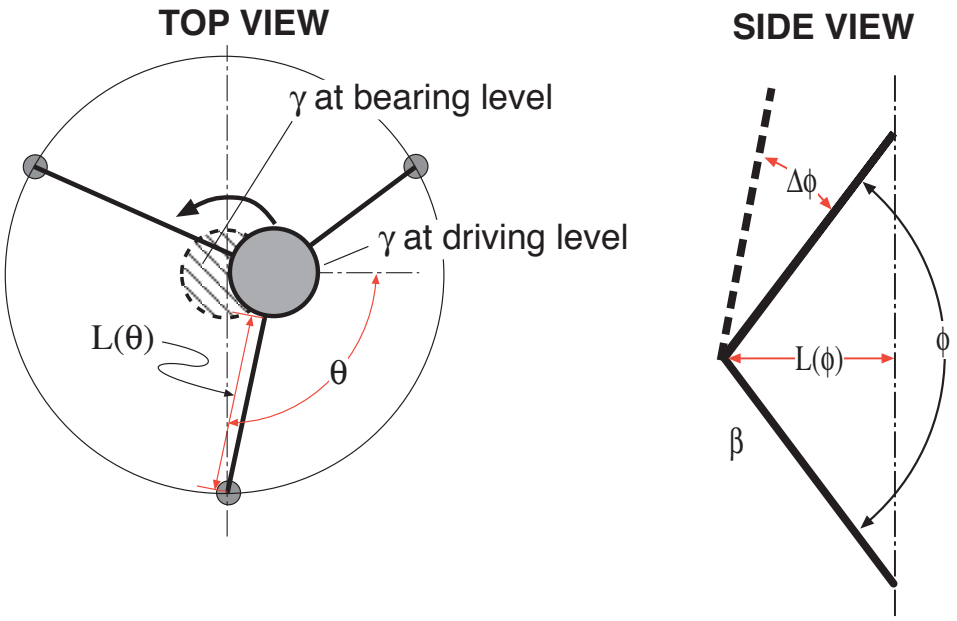

Figure 8 Coupling between the rotation angle, θ, of the γsubunit and the bending angle, ϕ, of the β subunit. In the left panel, the plane shown is perpendicular to the γaxis. In the right panel, the plane shown is parallel to the γ axis. See text for details.

We can calculate the potentials in a simpler way which is somewhat more intuitive. Because the change of the bending angle is small ($\Delta\phi \sim 30^\circ$), the length, L, of the top part of β projected onto the plane perpendicular to the γaxis is approximately a linear function of the bending angle, ϕ. Therefore, the active spring and the passive spring connecting the top and bottom parts of each β are also linear in the length, L, of the top part of the β projected onto the plane perpendicular to the γaxis. Of course, the linear relation between ϕ and L is an approximate one, as is the assumption that the springs are linear in ϕ. In this sense, it is no more reasonable to assume the springs are linear in terms of ϕ than to assume the springs are linear in terms of L. Thus we shall view the active and passive springs on each β as linear springs in the projected length L.

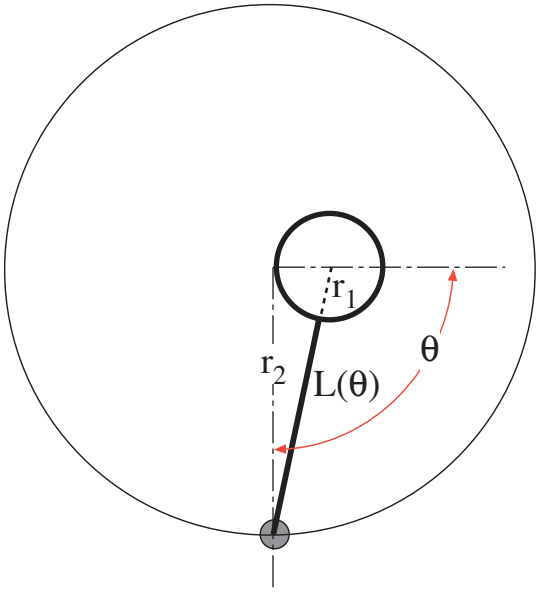

Figure 9 Mathematical calculation of the projected length, L, as a function of the rotation angle, θ.

As shown in Figure 9, the projected length, L, of the top part of β as a function of θ is given by

$$L(\theta) = \sqrt{r_1^2 + r_2^2 - 2\,r_1\,r_2\cos(\theta)} - r_1 \tag{30}$$

where $r_1 = 1$ nm and $r_2 = 4$ nm.

The elastic energy due to the passive spring as a function of θ is

$$E^P(\theta) = \frac{1}{2}k^P \cdot \left[\left(L(\theta) - L(0)\right) + \Delta L_{Precompress}\right]^2 - \frac{1}{2}k^P \cdot \left[\Delta L_{Precompress}\right]^2 \tag{31}$$

where the passive spring is pre-compressed by $\Delta L_{Precompress} = 4$ nm.

The elastic energy due to the active spring as a function of θ is

$$E^A(\theta) = \frac{1}{2}k^A \cdot \left[\left(L(\pi) - L(\theta)\right) + \Delta L_{Prestress}\right]^2 - \frac{1}{2}k^A \cdot \left[\Delta L_{Prestress}\right]^2 \quad (32)$$

where the active spring is prestressed by $\Delta L_{Prestress} = 4$ nm.

Viewing the passive and active springs in the direction of the projected length L simplifies the calculation of the potentials, and makes the bending motion of each β directly comparable to the linear motion of each piston in a three-cylinder engine.

The active spring is switched on only in states **T** and **D·P** while the passive spring is always engaged. The elastic energy in state **D** is due solely to the passive spring. However, the energy in state **E** requires an additional component because three experimental observations would be violated were we to model the elastic energy of the empty state by only the passive spring:

1. Rotation of γ driven by a proton flux is smaller in the absence of nucleotide than under normal synthesis conditions (Groth, et al., 1993).

2. Under hydrolysis conditions at low nucleotide concentrations rotation of γ proceeds stepwise, with 3 steps per revolution (Yasuda, et al., 1998).

3. The model should operate in reverse to synthesize ATP from ADP and phosphate.

To meet these requirements, we must modify the elastic potential in the empty state over what is provided by the passive spring. To do this we write the total free energies of each β for states **E, T, D·P** and **D** as

$$\begin{aligned}
E_E(\theta) &= & & E^P(\theta) + E^B_E(\theta) \\
E_T(\theta) &= E^A(\theta) + & E^P(\theta) + & E^B_T(\theta) \\
E_{DP}(\theta) &= E^A(\theta) + & E^P(\theta) + & E^B_{DP}(\theta) \\
E_D(\theta) &= & E^P(\theta) + & E^B_D(\theta)
\end{aligned} \quad (33)$$

In this equation, the superscripts A and P refer to the elastic potentials of the active and passive springs, respectively, as computed above. The superscript (B) represents the part of the elastic energy of the β caused by an additional interaction between the β and γ, and/or α. The additional elastic component in empty state, $\mathbf{E}^B_E$, makes empty βα pairs stiff; that is it creates a deep potential barrier against rotation of the γ subunit when three catalytic sites are empty. It also prevents the γ subunit from diffusing over a large angle when the catalytic site is empty, thus enforcing the observed stepping behavior.

In the hydrolysis direction, $\mathbf{E}^B_T$, $\mathbf{E}^B_{DP}$ and $\mathbf{E}^B_D$ are unnecessary. but in the synthesis direction all four additional terms ($\mathbf{E}^B_E$, $\mathbf{E}^B_D$, $\mathbf{E}^B_{DP}$ and $\mathbf{E}^B_T$) are required for (i) trapping ADP, (ii) trapping phosphate, (iii) forming ATP and (iv) releasing ATP (see Figure 1).

For example, in the synthesis direction, $\mathbf{E}^{B}_{E}$ raises the free energy on the **E** curve such that the transition **E** → **D** is promoted and the backward transition **D** → **E** is prohibited when the system is driven up the E curve by a mechanical torque.

Mathematical equations and numerical solutions

Langevin equation formulation

Since inertia is negligible, equating the viscous drag on the rotating γ to the other forces acting on it yields the Langevin equation (Doering, 1990; Risken, 1989),

$$\underbrace{\zeta \frac{d\theta}{dt}}_{\substack{\text{Viscous}\\ \text{torque on } \gamma}} = \underbrace{-\frac{dV(\theta;\mathbf{S})}{d\theta}}_{\substack{\text{Torque between}\\ \gamma \text{ and } \alpha_3\beta_3}} - \underbrace{T_L}_{\substack{\text{Load}\\ \text{torque}}} + \underbrace{\Im_B(t)}_{\substack{\text{Brownian}\\ \text{torque}}} \tag{34}$$

where ζ is the rotational drag coefficient, θ is the angular coordinate, V(θ; **S**) is the sum of the elastic energies of the three β's, T_L is the load torque, and $\Im_B$ is the Brownian torque due to thermal fluctuations. **S** = (β_1, β_2, β_3) represents the kinetic state of the three catalytic sites. **S** can take any of the $4^3 = 64$ possible kinetic states in the space

$$\{\, \mathbf{E, T, D{\cdot}P, D} \,\} \times \{\, \mathbf{E, T, D{\cdot}P, D} \,\} \times \{\, \mathbf{E, T, D{\cdot}P, D} \,\}$$

The probability of state **S** evolves according to kinetic equation (12), which we rewrite symbolically as

$$\frac{d}{dt}\mathbf{S} = \mathbf{K}(\theta) \cdot \mathbf{S} \tag{35}$$

To compute the torque generated by the F_1 motor, equation (34) must be solved simultaneously with the Markov process governing the kinetic transitions on the three catalytic sites (equation (35)).

Fokker-Planck equation formulation

In the Fokker-Planck formulation corresponding to equations (34) and (35), the F_1 motor is described by a vector function consisting of 64 probability density functions.

Let $\rho(\theta, t, \beta_{i-1}, \beta_i, \beta_{i+1})$ be the probability density that γ is at the angular position θ at time t, and the β's are in chemical states $\boldsymbol{\beta}_{i-1}$, $\boldsymbol{\beta}_i$ and $\boldsymbol{\beta}_{i+1}$, respectively. Define the probability density vector as:

$$\boldsymbol{\rho}(\theta, t) = \left.\begin{bmatrix} \rho(\theta, t, E, E, E) \\ \rho(\theta, t, E, E, T) \\ \rho(\theta, t, E, E, DP) \\ \rho(\theta, t, E, E, D) \\ \rho(\theta, t, E, T, E) \\ \rho(\theta, t, E, T, T) \\ \rho(\theta, t, E, T, DP) \\ \vdots \\ \rho(\theta, t, D, D, DP) \\ \rho(\theta, t, D, D, D) \end{bmatrix}\right\} 64 \text{ components} \tag{36}$$

This probability density vector evolves according to the convective diffusion equations

$$\frac{\partial \boldsymbol{\rho}(\theta, t)}{\partial t} = \frac{1}{\zeta}\frac{\partial}{\partial \theta}\left\{\left(\frac{d\mathbf{V}(\theta)}{d\theta} + T_L\right)\boldsymbol{\rho}(\theta, t)\right\} + D\frac{\partial^2 \boldsymbol{\rho}(\theta, t)}{\partial \theta^2} + \mathbf{K}(\theta)\cdot\boldsymbol{\rho}(\theta, t) \tag{37}$$

where $D = k_B T / \zeta$ is the rotational diffusion coefficient. The 64x64 transition matrix $\mathbf{K}(\theta)$ is defined in equation (12). The potential matrix $\mathbf{V}(\theta)$ is

$$\mathbf{V}(\theta) = \underbrace{\left.\begin{bmatrix} V_1(\theta) & & & & \\ & V_2(\theta) & & & \\ & & \ddots & & \\ & & & V_{63}(\theta) & \\ & & & & V_{64}(\theta) \end{bmatrix}\right\} 64 \text{ rows}}_{64 \text{ columns}} \tag{38}$$

where

$$\begin{aligned}
V_1(\theta) &= E_E(\theta + 2\pi/3) + E_E(\theta) + E_E(\theta - 2\pi/3) \\
V_2(\theta) &= E_E(\theta + 2\pi/3) + E_E(\theta) + E_T(\theta - 2\pi/3) \\
V_3(\theta) &= E_E(\theta + 2\pi/3) + E_E(\theta) + E_{DP}(\theta - 2\pi/3) \\
V_4(\theta) &= E_E(\theta + 2\pi/3) + E_E(\theta) + E_D(\theta - 2\pi/3) \\
V_5(\theta) &= E_E(\theta + 2\pi/3) + E_T(\theta) + E_E(\theta - 2\pi/3) \\
V_6(\theta) &= E_E(\theta + 2\pi/3) + E_T(\theta) + E_T(\theta - 2\pi/3) \\
&\vdots \\
V_{63}(\theta) &= E_D(\theta + 2\pi/3) + E_D(\theta) + E_{DP}(\theta - 2\pi/3) \\
V_{64}(\theta) &= E_D(\theta + 2\pi/3) + E_D(\theta) + E_D(\theta - 2\pi/3)
\end{aligned} \tag{39}$$

Numerical solution of Fokker-Planck equations

The dynamic and kinetic behaviors of the F_1 motor are governed by the Fokker-Planck equations (37). In this subsection, we discuss the numerical methods for solving them.

Equations (37) is a system with 64 coupled equations. The full construction of our numerical methods for general Fokker-Planck equations involves the analysis of the equations; details of the numerical analysis will be presented in a separate publication. Here we describe the numerical method for a model Fokker-Planck system with two coupled equations.

Consider the equations:

$$\begin{aligned}
\frac{\partial \rho_1}{\partial t} &= \underbrace{\frac{1}{\zeta}\frac{\partial}{\partial \theta}\left(\phi_1'(\theta)\rho_1\right) + D\frac{\partial^2 \rho_1}{\partial \theta^2}}_{\substack{\text{Probability flow}\\ \text{in the } \theta\text{-direction}}} \underbrace{-k_{12}(\theta)\cdot\rho_1 + k_{21}(\theta)\cdot\rho_2}_{\substack{\text{Probability flow in}\\ \text{the reaction direction}}} \\
\frac{\partial \rho_2}{\partial t} &= \underbrace{\frac{1}{\zeta}\frac{\partial}{\partial \theta}\left(\phi_2'(\theta)\rho_2\right) + D\frac{\partial^2 \rho_2}{\partial \theta^2}}_{\substack{\text{Probability flow}\\ \text{in the } \theta\text{-direction}}} \underbrace{-k_{21}(\theta)\cdot\rho_2 + k_{12}(\theta)\cdot\rho_1}_{\substack{\text{Probability flow in}\\ \text{the reaction direction}}}
\end{aligned} \tag{40}$$

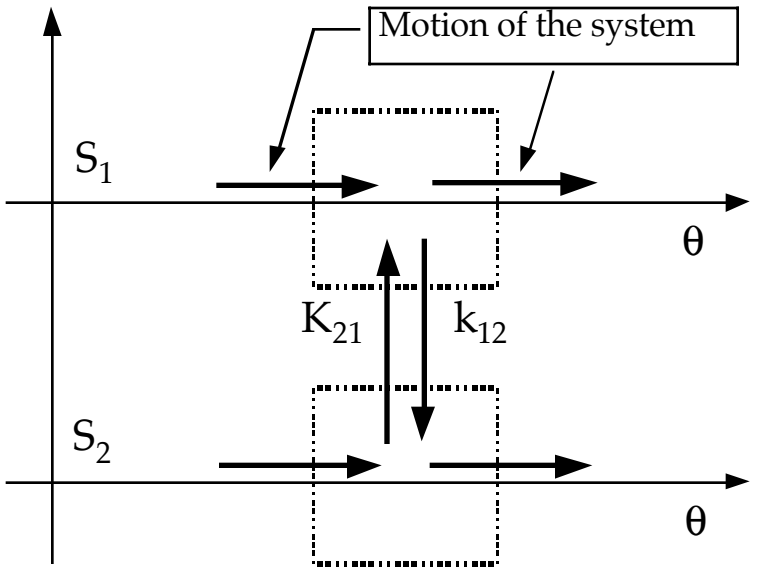

Figure 10 Probability flows in the θ-direction and the kinetic reaction direction.

The system governed by equations (40) has two kinetic states, denoted 1 and 2. $\rho_m(\theta, t)$ is the probability density that the system is at location θ at time t, and is in state m = 1,2. $\phi_m(\theta)$ is the potential of the system in state m. $k_{12}(\theta)$ is the transition rate from state 1 to

state 2, and $k_{21}(\theta)$ is the transition rate from state 2 to state 1. Equations (40) describe the conservation of probability at any location θ in each state. Figure 10 shows all in-flows and out-flows at a given location θ in states 1 and 2.

The numerical discretization is constructed as follows. First we divide the domain in the θ-direction into intervals of size Δθ, and call the center point of the n-th interval θ_n . Let $\rho_{m,n}(t)$ be the probability that the system is in the n-th interval at time t, and is in state m. Figure 11 shows the discrete probability in-flows and out-flows in both the θ and kinetic directions. The conservation of probability in the n-th interval in state m leads to differential difference equation of the form:

$$\begin{aligned}\frac{d\rho_{1,n}}{dt} &= F_{1,n-1/2}\cdot\rho_{1,n-1} - \left(B_{1,n-1/2} + F_{1,n+1/2}\right)\cdot\rho_{1,n} \\ &\quad + B_{1,n+1/2}\cdot\rho_{1,n+1} - k_{12,n}\cdot\rho_{1,n} + k_{21,n}\cdot\rho_{2,n} \\ \frac{d\rho_{2,n}}{dt} &= F_{2,n-1/2}\cdot\rho_{2,n-1} - \left(B_{2,n-1/2} + F_{2,n+1/2}\right)\cdot\rho_{2,n} \\ &\quad + B_{2,n+1/2}\cdot\rho_{2,n+1} - k_{21,n}\cdot\rho_{2,n} + k_{12,n}\cdot\rho_{1,n}\end{aligned} \tag{41}$$

where the kinetic transition rates in the n-th interval, $k_{12,n}$ and $k_{21,n}$, are given by

$$\begin{aligned}k_{12,n} &= k_{12}\left(\theta_n\right) \\ k_{21,n} &= k_{21}\left(\theta_n\right)\end{aligned} \tag{42}$$

$F_{m,n+1/2}$ is the forward jump rate from n-th interval to the (n+1)-th interval and $B_{m,n+1/2}$ is the jump rate from (n+1)-th interval back to the (n+1)-th interval. The jump rates $F_{m,n+1/2}$ and $B_{m,n+1/2}$ are constructed to preserve two important properties of the Fokker-Planck equations:

- The numerical method should maintain the principle of detailed balance. The ratio of the jump rates between two intervals is determined by the potential difference of the two intervals:

$$\frac{F_{m,n+1/2}}{B_{m,n+1/2}} = \exp\left(\frac{\phi_m\left(\theta_n\right) - \phi_m\left(\theta_{n+1}\right)}{k_B T}\right) \tag{43}$$

- For a uniform probability distribution, the net flux across $\theta_{n+1/2}$ in state m (the boundary between the n-th and (n+1)-th intervals) is proportional to the derivative of potential ϕ_m. When the derivative of potential ϕ_m is a constant, independent of n, this yields

$$\left(F_{m,n+1/2} - B_{m,n+1/2}\right)\cdot \Delta\theta = \frac{\phi_m(\theta_n) - \phi_m(\theta_{n+1})}{\zeta \cdot \Delta\theta} \tag{44}$$

Solving jump rates $F_{m,\,n+1/2}$ and $B_{m,\,n+1/2}$ from equations (43) and (44), we obtain

$$\begin{aligned} F_{m,n+1/2} &= \frac{D}{(\Delta\theta)^2}\cdot \frac{-\frac{\phi_m(\theta_n)-\phi_m(\theta_{n+1})}{k_B T}}{\exp\left(-\frac{\phi_m(\theta_n)-\phi_m(\theta_{n+1})}{k_B T}\right)-1} \\ B_{m,n+1/2} &= \frac{D}{(\Delta\theta)^2}\cdot \frac{\frac{\phi_m(\theta_n)-\phi_m(\theta_{n+1})}{k_B T}}{\exp\left(\frac{\phi_m(\theta_n)-\phi_m(\theta_{n+1})}{k_B T}\right)-1} \end{aligned} \tag{45}$$

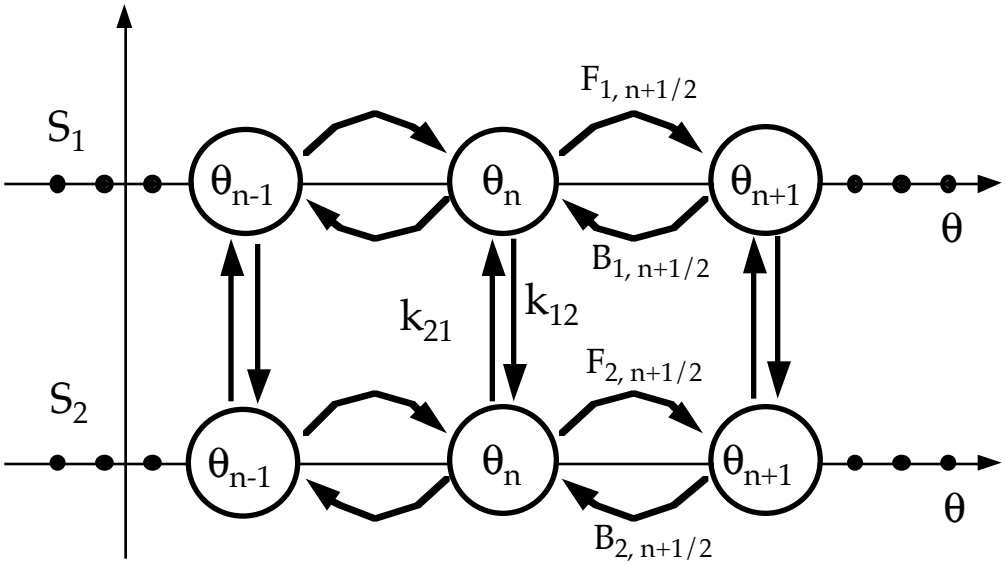

Figure 11 Conservation of probability in the n-th interval in states 1 and 2.

Once we know the transition rates in the kinetic direction and the discrete jump rates in the θ–direction, equations (41) are solved using a Crank-Nicolson scheme.

References

Abrahams, J., A. Leslie, R. Lutter, and J. Walker. 1994. Structure at 2.8Å resolution of F_1-ATPase from bovine heart mitochondria. *Nature* 370:621-628.

Boyer, P. 1993. The binding change mechanism for ATP synthase--some probabilities and possibilities. *Biochim. Biophys. Acta* 1140:215-250.

Doering, C. 1990. Modeling complex systems: Stochastic processes, stochastic differential equations, and Fokker-Planck equations. *In* 1990 Lectures in Complex Systems. L. Nadel, and D. Stein, editors. Addison-Wesley, Redwood City, CA. 3-51.

Elston, T., H. Wang, and G. Oster. 1998. Energy transduction in ATP synthase. *Nature* 391:510-514.

Groth, G., and W. Junge. 1993. Proton slip of the chloroplast ATPase: its nucleotide dependence, energetic threshold, and relation to an alternating site mechanism of catalysis. *Biochemistry* 32:8103-8111.

Kaibara, C., T. Matsui, T. Hisabori, and M. Yoshida. 1996. Structural asymmetry of F_1-ATPase cuased by the γ subunit generates a high affinity nucleotide binding site. *J. Biol. Chem.* 271:2433-2438.

Matsuno-Yagi, A., and Y. Hatefi. 1986. Kinetic Modalities of ATP Synthesis: Regulation by the Mitochondrial Respiratory Chain. *J. Biol. Chem.* 261:14031-14038.

Noji, H., R. Yasuda, M. Yoshida, and K. Kinosita. 1997. Direct observation of the rotation of F_1-ATPase. *Nature* 386:299-302.

Risken, H. 1989. *The Fokker-Planck Equation*. Springer-Verlag, New York.

Senior, A. 1992. Catalytic Sites of *Escherichia coli* F1-ATPase. *Journal of Bioenergetics and Biomembranes* 24:479-483.

Shirakihara, Y., A. Leslie, J. Abrahams, J. Walker, T. Ueda, Y. Sekimoto, M. Kambara, K. Saika, Y. Kagawa, and M. Yoshida. 1997. The Crystal Structure of the Nucleotide-Free $\alpha 3\,\beta 3$ Subcomplex of F1-ATPase from the Thermophilic Bacillus PS3 is a Symmetric Trimer. *Structure* 5:825-836.

Stryer, L. 1995. *Biochemistry*. W. H. Freeman, New York.

Weber, J., and A. E. Senior. 1997. Catalytic mechanism of F1-ATPase. *Biochim. Biophys. Acta* 1319:19-58.

Yasuda, R., H. Noji, K. Kinosita, F. Motojima, and M. Yoshida. 1997. Rotation of the γ Subunit in F_1-ATPase; Evidence That ATP Synthase Is a Rotary Motor Enzyme. *Journal of Bioenergetics and Biomembranes* 29:207-209.

Yasuda, R., H. Noji, K. Kinosita, and M. Yoshida. 1998. F_1-ATPase is a highly efficient molecular motor that rotates with discrete 120° steps. *Cell* 93:1117-1124.